Movement and Vertical Coupling of Adiabatic Baroclinic Tropical Cyclones*

LIGUANG WU AND BIN WANG+

Department of Meteorology, School of Ocean and Earth Science and Technology, University of Hawaii at Manoa, Honolulu, Hawaii

(Manuscript received 11 November 1999, in final form 20 October 2000)

ABSTRACT

The vertical coupling and movement of an adiabatic baroclinic tropical cyclone (TC) are investigated through two numerical experiments in which the TC is affected by either a vertical environmental shear or a differential beta drift. In both cases, the initial response of the symmetric vortex is to tilt in the vertical. In response to the vertical tilt, a three-dimensional asymmetric circulation with a typical radius of 100 km develops within the TC core region. In addition, the wavenumber-one potential vorticity (PV) anomalies develop with positive anomalies downtilt (uptilt) above (below) the maximum PV level in order to maintain a balanced state between the thermal and dynamical fields. On a beta plane, in contrast to the beta gyres, the mesoscale asymmetric circulation is a pair of counterrotating inner gyres centered at the radius of maximum wind. As a result, the resulting three-dimensional mesoscale asymmetric circulation, not the penetration flow, plays an important role in the vertical coupling of adiabatic baroclinic vortices. In both cases, the TC motion is not simply due to the advection of the symmetric PV component by the asymmetric (ventilation) flow. The horizontal advection of the asymmetric PV anomalies by the symmetric cyclonic flow and the vertical PV advection associated with the asymmetric vertical motion also considerably contribute to the TC motion. The latter two processes also play a critical role in the vertical coupling of the baroclinic TC due to the presence of the vertical PV gradient.

1. Introduction

Baroclinic tropical cyclone (TC) motion has been investigated through numerical models (e.g., Wang and Li 1992; Shapiro 1992; Wu and Emanuel 1993; Flatau et al. 1994; Jones 1995; Wang and Holland 1996a–c; Dengler and Reeder 1997). As in the barotropic case, most previous studies have related baroclinic TC motion to the asymmetric flow over the TC core region. For instance, Wang and Li (1992) suggested that the beta-drift velocity of an initially symmetric baroclinic vortex is approximately equal to the geostrophic flow implied by asymmetric pressure gradients at the surface vortex center. By defining TC motion as the vortex movement in the middle layer, Shapiro (1992) argued that the TC translation in his three-layer model arises from the flow between the asymmetric gyres in the middle layer. In a tilted three-dimensional vortex capped with upper-level negative potential vorticity (PV) anomalies, Wu and Emanuel (1993) proposed that the upper-level negative PV anomalies could affect the low-level vortex motion through the so-called asymmetric penetration flows. In an adiabatic model, Wang and Holland (1996a) found that the vortex movement is determined by both the asymmetric flow over the vortex core associated with beta gyres and the asymmetric flow associated with vertical projection of tilted PV anomalies at the upper levels.

These studies also show that, without heating, a baroclinic TC can move as a whole in the presence of moderate vertical differential beta drift or environmental shears. The proposed mechanisms for the vertical coupling remain controversial. Wang and Li (1992) and Flatau et al. (1994) suggested that the vertical circulation may play an important role in the vertical coupling. On a beta plane, as illustrated by Elsberry (1995), the upward decreasing tendency in the beta drift tends to tilt the vortex eastward and equatorward with height in the Northern Hemisphere. In response to the vertical tilt, a warming (cooling) anomaly develops ahead of (behind) the vortex center with adiabatic descending (ascending) motion ahead of (behind) the vortex center. The resulting deep vertical motion couplet establishes vertical coupling within the vortex by inducing a low-level negative (upper-level positive) vorticity tendency at the lower (upper) levels. On the other hand, Jones (1995) and Wang and Holland (1996a) argued that the mesoscale asymmetric vertical circulation is not enough to account for the vertical coupling in their models. In-

* School of Ocean and Earth Science and Technology Publication Number 5427, and International Pacific Research Center Publication Number IPRC-88.

+ Additional affiliation: International Pacific Research Center, University of Hawaii at Manoa, Honolulu, Hawaii.

Corresponding author address: Dr. Bin Wang, Department of Meteorology and International Pacific Research Center, University of Hawaii at Manoa, 2525 Correa Road, Honolulu, HI 96822.
E-mail: bwang@soest.hawaii.edu

stead, they attributed the vertical coupling to penetration flows at the different vertical levels.

Understanding the baroclinic TC motion includes understanding not only the processes that determine three-dimensional TC motion but also the mechanism by which a baroclinic TC maintains its vertical coherent structure. Although both aspects have been investigated by introducing vertical environmental shears (e.g., Wu and Emanuel 1993; Flatau et al. 1994; Jones 1995; Wang and Holland 1996b) or the differential beta drift (e.g., Wang and Li 1992; Shapiro 1992; Wang and Holland 1996a), lack of quantitative analysis hinders us from clarifying the ambiguities in these aspects. First, due to the vertical coupling, it is not adequate to take the contribution of a certain physical process to the vortex movement at a single level as its contribution to the whole TC motion. Second, both observational (Wu and Emanuel 1995a,b) and numerical (Wang and Holland 1996a–c; Bender 1997) studies showed the existence of significant vertical shears in the asymmetric flows in the TC core region, while a three-dimensional TC moves as a whole. As a result, the estimated contribution of the asymmetric flow over the TC core strongly depends upon how the asymmetric steering flow is calculated. Third, Wu and Wang (2000) recently showed that a TC, treated as a positive PV anomaly relative to its environment, tends to move to the region with maximum PV tendency. In other words, the TC motion is not necessarily determined by the asymmetric flow averaged over the TC core region. All the physical processes that contribute to the wavenumber-one component of the PV tendency can affect TC motion.

In this study, we focus in particular on the movement and vertical coupling of adiabatic baroclinic TCs. The following specific issues are addressed. 1) How important is the steering of the asymmetric flow over the TC center to the TC motion? 2) How do other physical processes contribute to the baroclinic TC motion? 3) How does a baroclinic vortex maintain its coherent structure when it is affected by environmental vertical shears or differential beta drift? In order to address these questions, the PV tendency diagnostic approach (Wu and Wang 2000) is applied to the output of numerical experiments. The numerical experiments and the corresponding TC motion are described in section 2. The contributions of various physical processes to TC motion are assessed in section 3. Since TC motion and the vertical coupling are essentially associated with the asymmetric circulation within a TC, a discussion of the development of the asymmetric circulation is presented in section 4. The physical mechanism for the vertical coupling is discussed in section 5, followed by a summary in section 6.

2. Numerical experiments and vortex motion

The hurricane model used in this study is the same as that used by Wu and Wang (2000). The model, designed by Wang (1998), consists of 201 $\times$ 201 grid points with a uniform spacing of 25 km and 16 vertical layers in the σ coordinates. In this study, two adiabatic numerical experiments are designed by focusing on the influence of environmental shears and differential beta drift on baroclinic TC motion, respectively. The first experiment (E1) is run on an f plane in an environmental flow with a westerly shear. The easterly environmental flow decreases linearly from -4 m s^{-1} at the surface to 0 m s^{-1} at the top of the model. The second experiment (E2) is run on a beta plane in a resting environment. Both experiments begin with an initially symmetric baroclinic vortex. Its intensity decreases with height, but without anticyclonic circulation at the upper levels. The maximum wind, which is 25 m s^{-1} at the lowest level, is located at a radius of 100 km.

The vortex center is defined as the location of the maximum PV. The center positioning is carried out at each vertical level in order to avoid unrealistic asymmetric circulation arising from the variation of the TC center with height. Since the vortex in E1 is embedded in an easterly environmental flow, the overall direction of vortex motion is westward. Under the influence of the westerly environmental shear, however, the vortex in E1 tilts with height (Fig. 1a). It first tilts northeastward with height, and then northwestward. Its center at about 440 kPa first moves northwestward, whereas its surface center moves southwestward. The surface center is located about 947 km to the west and 95 km to the south of its initial position after a 72-h integration. As an adiabatic beta-drift problem, the surface center of the vortex in E2 moves about 253 km to the west and 316 km to the north (Fig. 1b). The average speed is 1.6 m s^{-1} with a direction of 321°. This agrees with previous numerical studies (e.g., Wang and Li 1992; Flatau et al. 1994; Wang and Holland 1996a) and resembles the observational studies (Carr and Elsberry 1990; Franklin et al. 1996).

It is worthy to note that the vertical tilt of the vortices in E1 and E2 does not necessarily increase with time. In addition, as shown in Figs. 1 and 2, the vertical tilt is much smaller from the surface to the middle level than above the midlevel. In E1, the tilt between 660 hPa and the surface is within 50 km. In E2, the circulation at these two levels is actually well aligned in the vertical and the tilt between 660 and 440 hPa is also within 50 km. This suggests that, consistent with the previous studies (Wang and Li 1992; Flatau et al. 1994; Jones 1995; Wang and Holland 1996a), there exists a physical mechanism by which the baroclinic TC maintains its coherent vertical structure.

3. Contributions of physical processes to TC motion

In this section, we assess the contributions of various physical processes to the three-dimensional TC motion in E1 and E2. First, the influence of physical processes

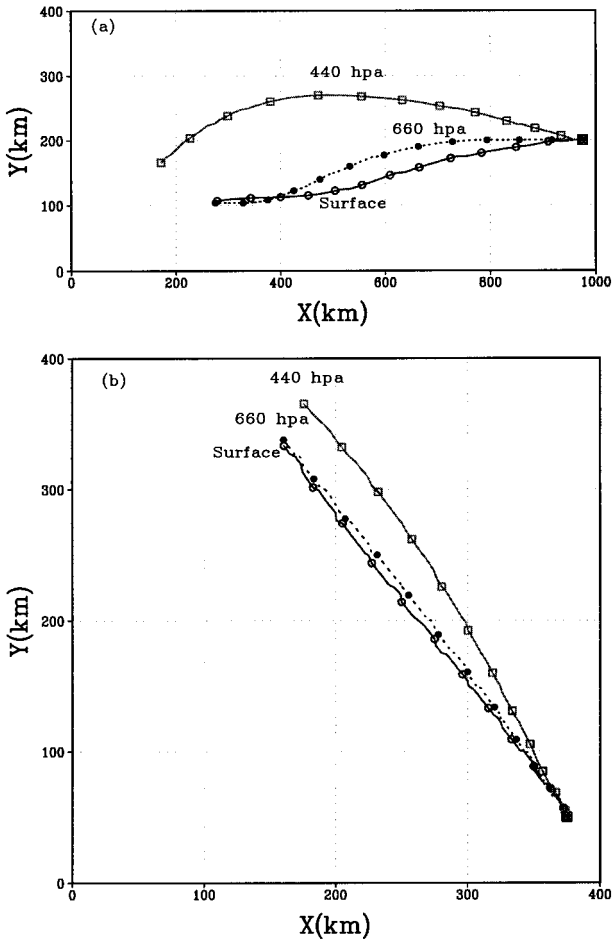

FIG. 1. The 72-h tracks of the vortex centers of different levels in (a) E1 and (b) E2, with 6-h positions indicated by circles, closed dots, and open squares for surface, 660 hPa, and 440 hPa, respectively. The initial position is indicated by a large square.

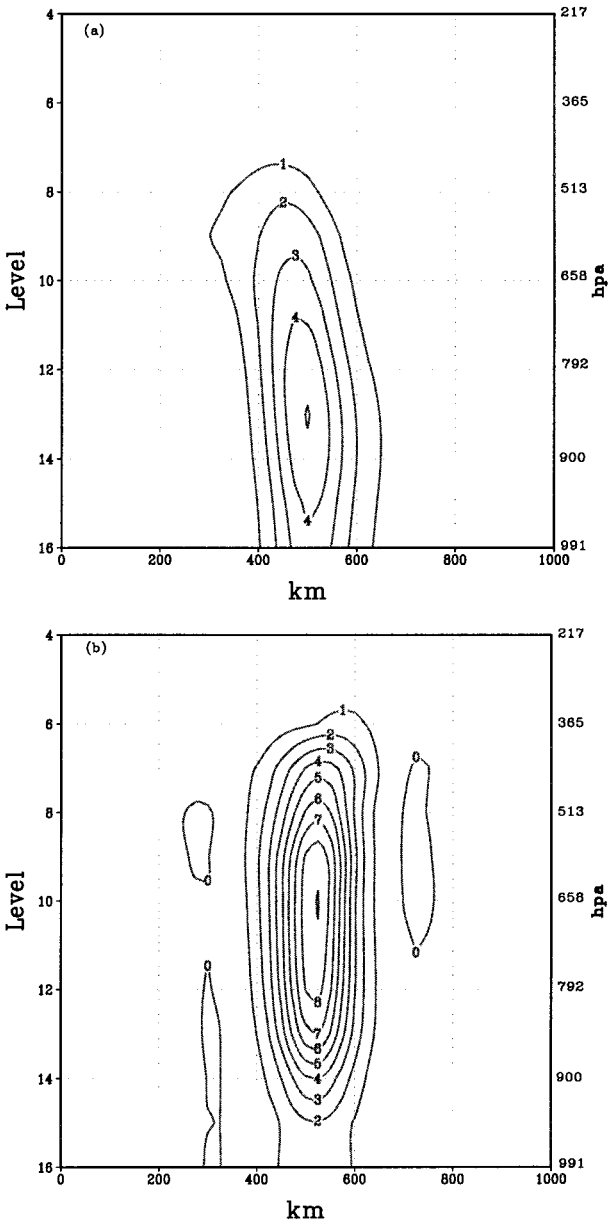

FIG. 2. The west–east PV cross section at 48 h in (a) E1 and (b) E2, with the contour intervals of 1.0 PVU.

on the vortex motion at each vertical level is identified using the PV tendency diagnostic approach proposed by Wu and Wang (1999, 2000). They showed that an adiabatic vortex at a level moves to the region with the maximum wavenumber-one component of the PV tendency. That is,

$$\left(\frac{\partial P}{\partial t}\right)_1 = -\mathbf{C}\cdot\nabla P_s, \tag{1}$$

where P and P_s are PV and the symmetric component of PV, respectively. Note that $\mathbf{C}$ is the vortex speed at a vertical level. Subscript 1 denotes the wavenumber-one component. In this case, the contributions of individual physical processes to the vortex motion at a level are equivalent to their contributions to the wavenumber-one component of the PV tendency. If the gradient of P_s and the PV tendency are given in Eq. (1), the total and fractional contributions from various physical processes can be estimated in terms of the TC motion speed by the least squares method (Wu and Wang 2000). In the adiabatic case, the average error of this method is about 0.2 m s^{-1}. In this section, we first look at the contributions of various physical processes to the two-dimensional vortex motion at each level (hereafter the vortex motion), and then the three-dimensional TC motion (hereafter the TC motion).

a. Contributions to the vortex motion

In an adiabatic case without friction, the wavenumber-one component of the PV tendency equation can be written as

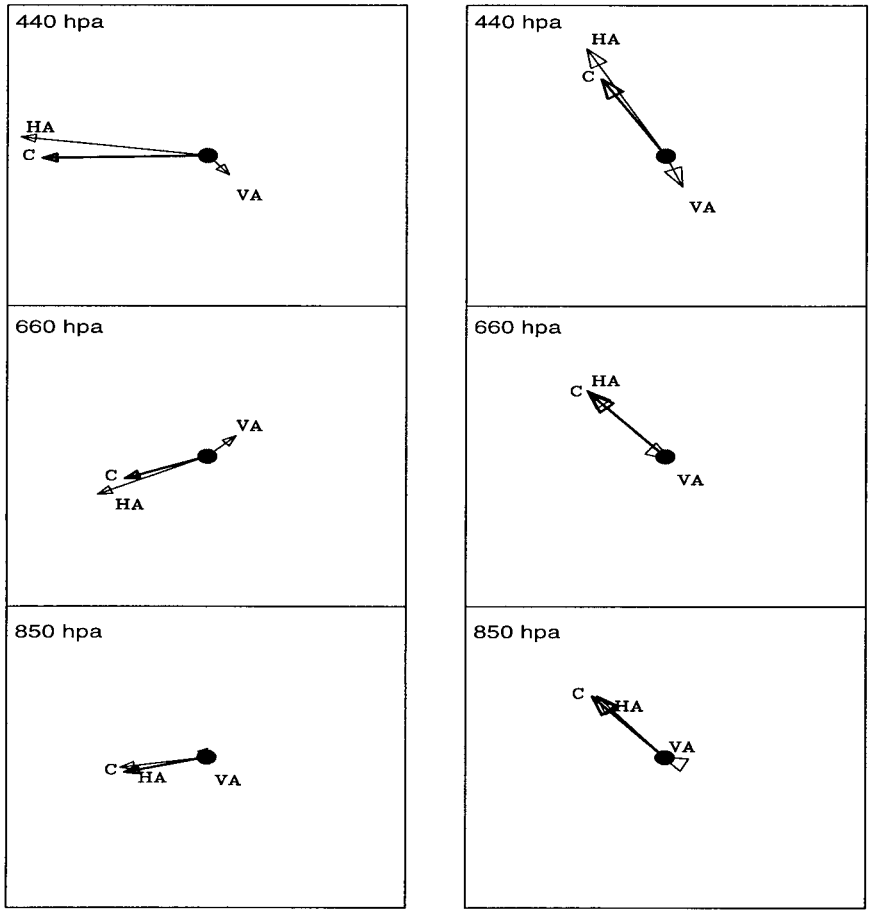

FIG. 3. Contributions of horizontal advection (HA), vertical advection (VA), and their sum (C) denoted by arrows at 48 h. Note that the scale in the left panels is different from that in the right panels. The contributions of HA are 4.9, 3.2, and 2.3 m s^{-1} at 440, 660, and 850 hPa in (left panels) E1, respectively. In (right panels) E2, the contributions of HA are, respectively, 0.9, 2.4, and 2.6 m s^{-1} at these levels.

$$\left(\frac{\partial P}{\partial t}\right)_1 = \Lambda_1\left\{-\mathbf{V}\cdot\nabla P - \dot{\sigma}\frac{\partial P}{\partial \sigma}\right\}, \qquad (2)$$

where $\mathbf{V}$ and $\dot{\sigma}$ are the horizontal and vertical velocities in the σ coordinates; Λ_1 denotes an operator to obtain the wavenumber-one component. In Eq. (2), two physical processes are responsible for the PV redistribution. One is the horizontal PV advection (HA), and the other is the vertical PV advection (VA). These two processes result in the local PV change with time, and thus, the vortex motion. In terms of the TC motion speed, Fig. 3 shows the estimated contributions of these two processes at different levels in E1 and E2, respectively. As demonstrated by Wu and Wang (2000), the estimated contributions are independent of the domain size if the domain is larger than 150 km $\times$ 150 km, suggesting that such a domain can provide sufficient information for accurately estimating the contributions. This is because the PV anomaly associated with a TC is highly localized and is primarily confined in a radius of about 200 km (Fig. 2). We define a domain as a square area of 400 km $\times$ 400 km in all the following calculations.

In both cases, the vortex motion is primarily determined by the influence of HA, whereas the VA plays a secondary role in the vortex motion. The total contributions of these two processes at 660 and 850 hPa in E1 and at the three levels in E2 are very similar, respectively. Figure 3 suggests that the VA can play a significant role in maintaining a uniform vortex speed in the vertical. In order to maintain such a uniform vortex speed, in E1 it leads to a northeastward motion component at 660 hPa. In E2 it leads to a southeast motion component at 440 hPa. Furthermore, the contribution of VA to the vortex motion is closely associated with the vertical tilt. In E2, for example, it is negligibly small because of the absence of the vertical tilt at the middle and lower levels.

If the TC circulation is dominated by the symmetric and wavenumber-one components, the wavenumber-one

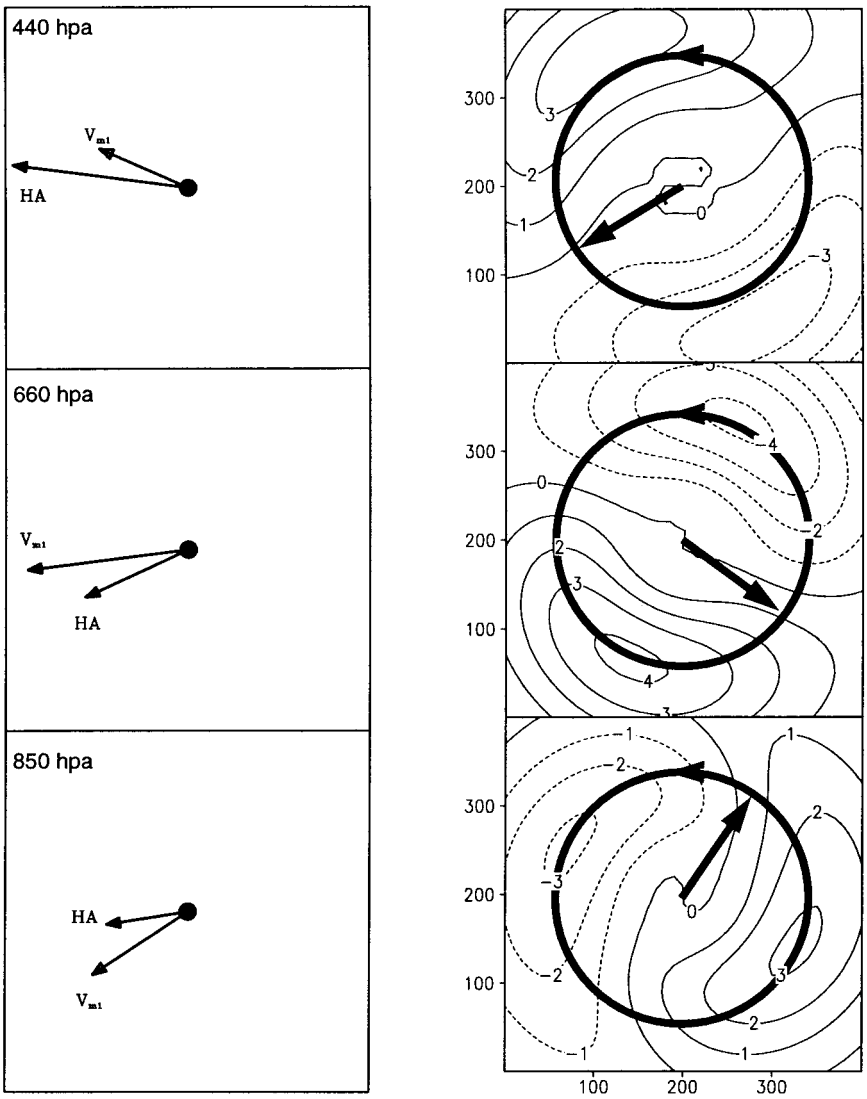

FIG. 4. Contributions of horizontal advection (HA) and the asymmetric flow steering at 440, 660, and 850 hPa at 48 h in (left panels) E1, and (right panels) the corresponding wavenumber-one PV components at these levels with intervals of 1.0×10^{-8} K kg^{-1} m^2 s^{-1}. The thick arrows show the directions of contribution of AASF, and the circles denote the symmetric cyclonic circulation.

component of HA can be further partitioned into two components as follows:

$$\Lambda_1(-\mathbf{V}\cdot\nabla P)\approx -\mathbf{V}_1\cdot\nabla P_s - \mathbf{V}_s\cdot\nabla P_1, \qquad (3)$$

where $\mathbf{V}_s$ and $\mathbf{V}_1$ are the symmetric and wavenumber-one components of the wind vector at a certain level, respectively. The effects of the large-scale steering and the secondary steering in the beta-drift problem are included in the first term on the right-hand side of Eq. (3), the advection of the symmetric PV component by the asymmetric flow (ASAF). Note that, unlike the traditional steering concept, the influence of ASAF on the vortex motion is also associated with the horizontal gradient of the symmetric PV component, P_s. Since the horizontal PV gradient is primarily confined within a radius of 200 km (Fig. 2), the $\mathbf{V}_1$ in the inner core region effectively steers the vortex. This agrees with the studies by Marks et al. (1992) and Franklin et al. (1996). With airborne Doppler radar data, they found that the asymmetric flow averaged within 3° latitude from a TC center is best correlated with storm motion.

In terms of TC motion speed, the contribution of ASAF can be approximately estimated by calculating the mean wavenumber-one flow ($\mathbf{V}_{m1}$) over a domain within a radius of 200 km. For comparison with the contributions of HA and VA, the domain is 400 km $\times$ 400 km. Figures 4 and 5 (left panels) compare the contribution of HA and the areal mean wavenumber-one

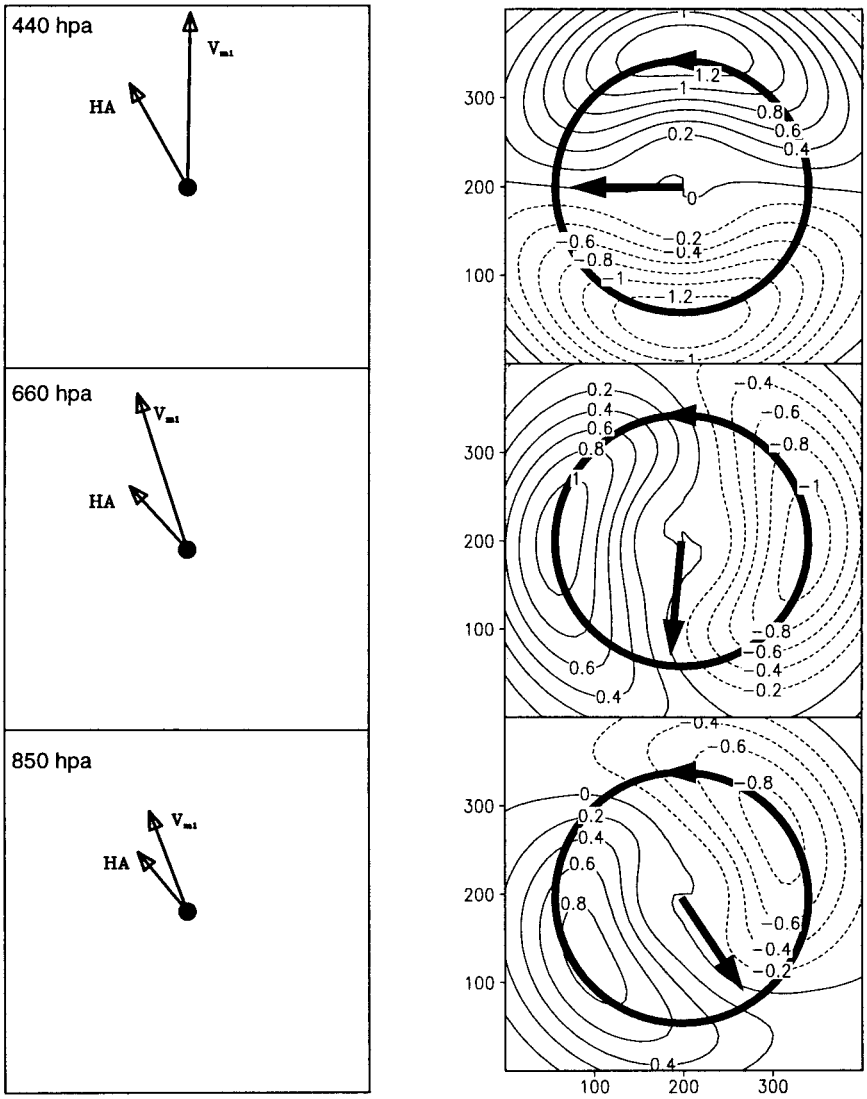

FIG. 5. Contributions of horizontal advection (HA), and the asymmetric flow steering at 440, 660, and 850 hPa at 48 h in (left panels) E2, and (right panels) the corresponding wavenumber-one PV components at these levels with intervals of 1.0×10^{-8} K kg^{-1} m^2 s^{-1}. The thick arrows show the directions of contribution of AASF, and the circles denote the symmetric cyclonic circulation.

flow ($\mathbf{V}_{m1}$) in E1 and E2, respectively. In both cases, $\mathbf{V}_{m1}$ is significantly different from the contribution of HA.

The HA associated with the second term on the right-hand side of Eq. (3), the advection of the asymmetric PV component by the symmetric flow (AASF), can be inferred from the wavenumber-one PV fields shown in Figs. 4 and 5 (right panels). In Fig. 4, the maximum positive asymmetric PV advection caused by the cyclonic symmetric flow shown by the thick circles is toward the southwest, southeast, and northeast of the vortex centers at 440, 660, and 850 hPa, respectively. According to Wu and Wang (2000), the resulting PV tendencies produce southwestward, southeastward, and northeastward motion vectors at these levels, respectively, as shown by the thick arrows (the right panels). The combination of the contributions from AASF and ASAF can approximately account for the influence of HA in E1 (the left panels of Fig. 4). In E2 (Fig. 5), as shown by the thick arrows, the AASF leads to westward, southward, and southeastward motion vectors at 440, 660, and 850 hPa, respectively. The sum of the influences of AASF and $\mathbf{V}_{n1}$ can also approximately account for the contribution of HA. Therefore, both ASAF and AASF contribute to the vortex motion at a certain level.

Similarly, the VA can be partitioned into two terms: the advection of the symmetric PV component by the azimuthally asymmetric vertical motion $[-\dot{\sigma}_1(\partial P_s/\partial_\sigma)]$

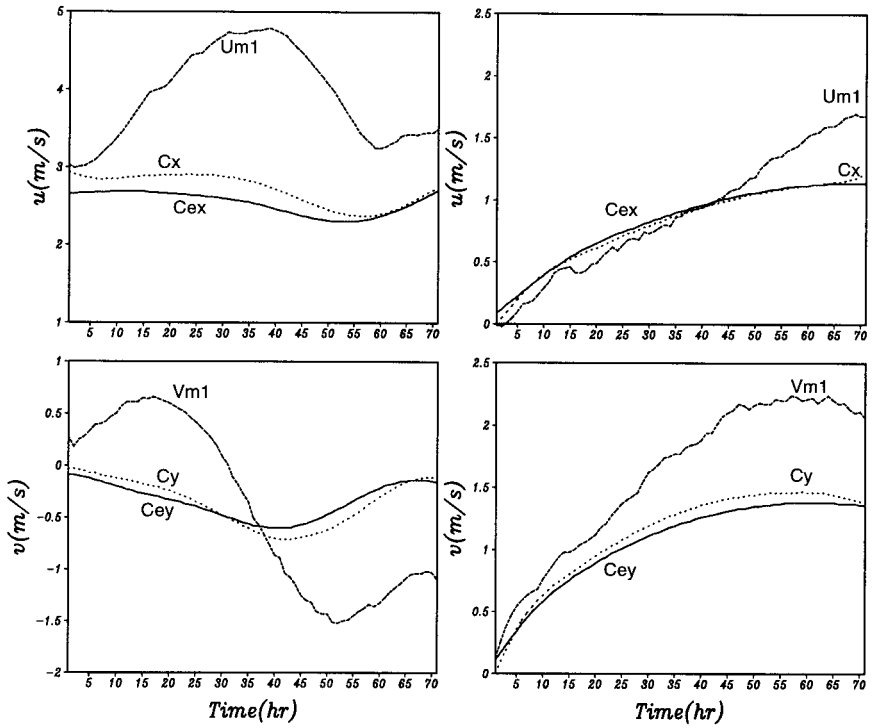

FIG. 6. Time series of the zonal (westward) and meridional (northward) vertical mean TC speeds calculated from TC center positions (**C**, dotted) and PV tendency ($\mathbf{C}_e$, solid), in comparison with the vertical mean asymmetric flow ($\mathbf{V}_{m1}$, dashed) in (left panels) E1 and (right panels) E2.

and the advection of asymmetric PV component by the symmetric vertical motion $[-\dot{\sigma}_s(\partial P_1/\partial_\sigma)]$. The second term is negligible compared with the first term for both E1 and E2. In other words, the influence of VA is dominated by the advection of symmetric PV component by the asymmetric vertical motion $[-\dot{\sigma}_1(\partial P_s/\partial\sigma)]$.

b. Contributions to the TC motion

Now we consider the three-dimensional TC motion. According to the above analysis, the contributions of various processes to the vortex motion are also determined by the PV gradients. This means that these processes can contribute to the TC motion only in the region with significant PV gradients. Therefore, the vertical mean motion speed should be calculated based on the vertical extent of the PV anomaly associated with a TC. As shown in Fig. 2, the TCs, as positive PV anomalies relative to their environment, primarily extend from the surface to 513 hPa in E1 and from the surface to 365 hPa in E2, respectively. Figure 6 shows the vertical mean TC speeds estimated, respectively, from the vortex center positions (dotted) and PV tendency (solid) in E1 and E2. We also calculate the vertical mean speed of the asymmetric flow over the same vertical extent. As shown in Fig. 6, the TC motion speed is very close to that estimated from the PV tendency, while it is significantly different from the vertical mean speed of the asymmetric flow ($\mathbf{V}_{m1}$).

Since the contribution of vertical PV advection to the vortex motion is relatively small (Fig. 3), it cannot account for the difference between the $\mathbf{V}_{m1}$ and the TC speed. It is suggested that the difference primarily arises from the contribution of AASF. Therefore, three-dimensional adiabatic TC motion is primarily determined by ASAF, AASF, and the vertical advection of the symmetric PV component by the asymmetric vertical motion. We cannot use only the asymmetric flow averaged over the TC core region to account for the motion of an adiabatic baroclinic TC.

4. Development of the mesoscale asymmetric circulation (inner gyres)

From the above analysis, we have demonstrated that three processes primarily contribute to the wavenumber-one component of the PV tendency: ASAF, AASF, and the vertical advection of the symmetric PV component by the asymmetric vertical motion $[-\dot{\sigma}_1(\partial P_s/\partial_\sigma)]$. Retaining these terms in Eq. (2) and combining Eq. (1) with Eq. (2) yield

$$\dot{\sigma}_1\frac{\partial P_s}{\partial\sigma} = -\mathbf{V}_s\cdot\nabla P_1 - (\mathbf{V}_1 - \mathbf{C})\cdot\nabla P_s. \qquad (4)$$

As suggested by Eq. (4), a three-dimensional asymmetric circulation ($\mathbf{V}_1$, σ_1) develops within an initially symmetric TC, and the TC motion is closely associated

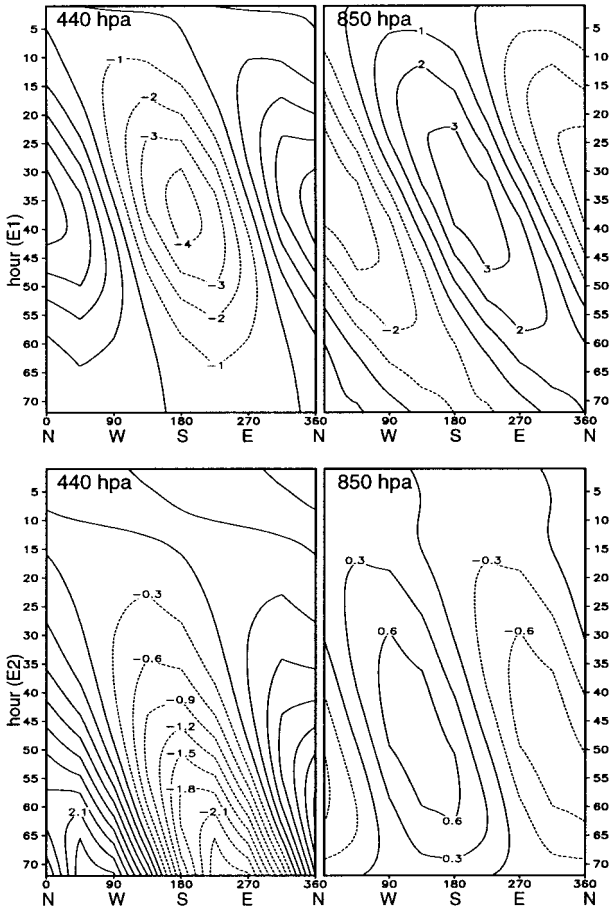

FIG. 7. The time evolution of the asymmetric PV component ($\times 1.0^6$ K kg^{-1} m^2 s^{-1}) at levels 7 (440 hPa) and 13 (850 hPa) in E1 and E2. The vertical coordinate denotes time (h) and the horizontal coordinate denotes the direction measured cyclonically from due north.

with the asymmetric circulation. In this section, we examine how the asymmetric circulation develops within an initially symmetric baroclinic vortex.

a. Asymmetric potential vorticity fields

Under the influence of the vertical environmental shear or differential beta drift, an asymmetric PV component develops within the initially symmetric vortices (Figs. 4 and 5). Note that the phase of the wavenumber-one PV varies with height. In E1 (Fig. 4), the positive PV anomaly is located to the northwest of the vortex center at 440 hPa, but to the southeast of the vortex center at 850 hPa. Such a vertical phase difference also occurs in E2. As shown in Fig. 5, the positive PV anomaly is to the north of the vortex center at 440 hPa, but to the southwest of the vortex center at 850 hPa.

Figure 7 further shows the evolution of the asymmetric PV component on a circle of 100-km radius from the vortex center, where the asymmetric PV anomaly approximately reaches its maximum or minimum. The direction is measured cyclonically from due north. As shown in this figure, the asymmetric PV component rotates cyclonically with time, but very slowly compared with cyclonic flows of the vortex. At the beginning ($t = 0$), the positive PV anomaly is located to the south of the vortex center at all the levels in E1 due to the westerly shear of the environmental flow. After the first several hours (say, $t = 5$), the positive anomaly is relocated to the southwest (northeast) of the vortex center at 850 hPa (440 hPa). Likewise, due to the beta effect in E2, the positive PV anomaly is initially located to the north of the vortex center at all the levels. With the development of the beta gyres, the phase of the asymmetric PV pattern quickly adjusts. Around 12 h, the positive PV anomaly is to the west (east) of the vortex center at 850 hPa (440 hPa).

Evidence shows that the asymmetric PV anomaly pattern is associated with the vertical tilt of the baroclinic vortices. First, as shown in Fig. 1, the lower- and upper-level centers rotate cyclonically with respect to the middle-level center. This cyclonic rotation is consistent with the cyclonic rotation of the phase in the wavenumber-one PV fields as shown in Fig. 7. Second, the magnitudes of the asymmetric PV anomalies are also related to the vertical tilt. In E1, the maximum tilt around 36 h coincides with the maximum magnitudes of the asymmetric PV anomalies, as seen in Fig. 7. In E2, the vertical tilt is smaller than that in E1, and the magnitudes of the asymmetric PV anomalies are also smaller. It is interesting to note that the tilt between the surface and 660 hPa in E2 reaches its maximum around 48 h, and so does the magnitude of the asymmetric PV anomaly. In addition, with the increasing tilt between 440 and 660 hPa, the magnitude of the asymmetric PV anomaly at 440 hPa keeps increasing. Third, the configuration of the PV anomalies is directly associated with the tilt direction. At the upper levels, the positive (negative) anomaly is on the down-tilt (up-tilt) side of the vortex center. At the lower levels, the positive (negative) anomaly is on the up-tilt (down-tilt) side of the vortex center. For example, in response to the northeastward tilt in E1 around 12 h (Fig. 1), a positive (negative) PV anomaly is located to the northeast (southwest) of the vortex center at 440 hPa, whereas a positive (negative) PV anomaly is found to the southwest (northeast) of the vortex center at 850 hPa (Fig. 7).

The response of an azimuthally symmetric PV anomaly to vertical environmental shears has been investigated recently. In a semibalance model, Raymond (1992) showed that the initially symmetric PV anomaly tilts in the plane of the shear, with an anomalously warm (cool) region up-shear (down-shear) of the vortex core. In Jones' (1995) study, a similar potential-temperature pattern is observed. As argued by Jones, the temperature anomaly is required for the flow to remain balanced. In order to demonstrate this, an initially symmetric PV anomaly is tilted by gradually shifting its wind field in the vertical. The potential temperature field can be com-

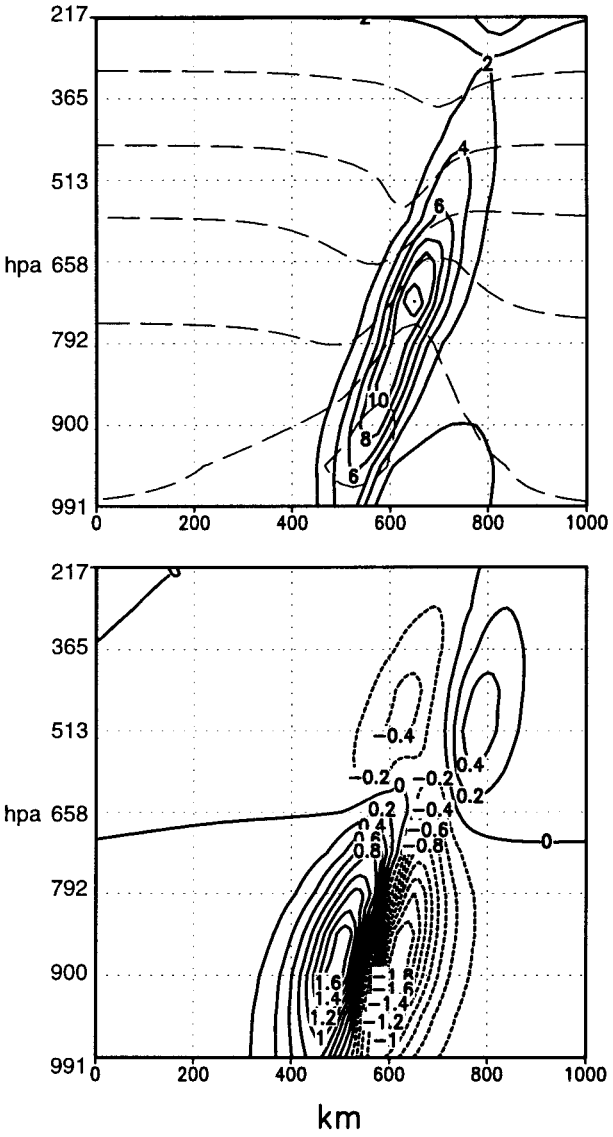

FIG. 8. (top) The vertical profiles of potential temperature (thin) and PV (thick) of a tilted vortex, which is symmetric before tilted. (bottom) The corresponding asymmetric PV profile.

puted (Wang 1995) based on the nonlinear balance equation. In agreement with Raymond (1992) and Jones (1995), the resulting isentropes are lowered (lifted) up-tilt (down-tilt) of the vortex center (Fig. 8). Since the isentropes are also the constant PV surfaces, the PV surfaces are lowered (lifted) up-tilt (down-tilt) of the vortex center. As shown in Fig. 8, the PV field has its maximum at the middle levels. The lifted PV surfaces lead to a positive (negative) PV anomaly at the upper (lower) levels, and the lowered PV surfaces lead to a negative (positive) PV anomaly at the upper (lower) levels. The resulting PV anomalies are out of phase at the lower and upper levels. Therefore, the asymmetric PV fields are primarily the result of the vertical tilt of an adiabatic baroclinic vortex.

Note that the relationship between the vortex tilt and the resulting PV anomalies at the middle levels can be complicated. Experiments show that the maximum symmetric PV occurring at lower levels leads to weaker PV anomalies at the upper levels. In this case, the level of the phase transition of the asymmetric PV anomalies does not coincide with the level of the maximum symmetric PV. In Fig. 8, the phase transition occurs between 513 and 658 hPa, whereas the maximum symmetric PV is located between 658 and 792 hPa. Therefore, as shown in Fig. 4, the asymmetric PV field at 660 hPa does not seem to be associated with the vertical tilt in E1. In addition, the direction of vortex tilt varies with height, especially in E1. As shown in Fig. 1, at 48 h the vortex tilts northwestward at the lower levels and then northward at the upper levels. For these reasons, the vortex at 660 hPa tilts northwestward, whereas the positive (negative) anomaly is located to the southwest (northeast) of the vortex center.

b. Asymmetric vertical motion and potential-temperature fields

The development of the vertical motion can be understood in terms of the resulting PV anomalies discussed above because an adiabatic air parcel moves on a constant PV surface. In order to understand the resulting vertical motion, two mechanisms should be considered here as suggested by Eq. (4). Let us illustrate these mechanisms in E2. The first mechanism is indicated by the first term on the right-hand side of Eq. (4). At 48 h, the positive (negative) PV anomaly at 440 hPa is located to the north (south) of the vortex center (Fig. 5). Since the symmetric PV component decreases with height (increase with σ) at this level (Fig. 2), the superposition of the positive (negative) PV anomaly leads to a rise (fall) of PV surfaces. As an air parcel moves toward the raised (lowered) PV surface with the symmetric cyclonic flow, it must ascend (descend). As a result, the maximum upward (downward) motion occurs to the east (west) of the vortex center. At 850 hPa, on the other hand, the symmetric PV component increases with height (decrease with σ) (Fig. 2), the superposition of the positive (negative) PV anomaly results in the fall (rise) of the total PV surfaces to the southwest (northeast) of the vortex center. The maximum upward (downward) motion occurs to the southeast (northwest) of the vortex center as an air parcel moves with the symmetric cyclonic flow.

The second mechanism for the development of the asymmetric vertical motion is indicated in the second term on the right-hand side of Eq. (4), which is related to the relative flow ($\mathbf{V}_1 - \mathbf{C}$) and the PV gradient in the radial direction. The maximum PV is located at the vortex center. For an air parcel that moves toward the vortex center with a smaller PV value, it must ascend (descend) if the symmetric PV component increases (decreases) with height at the upper- (lower-) levels. In E2,

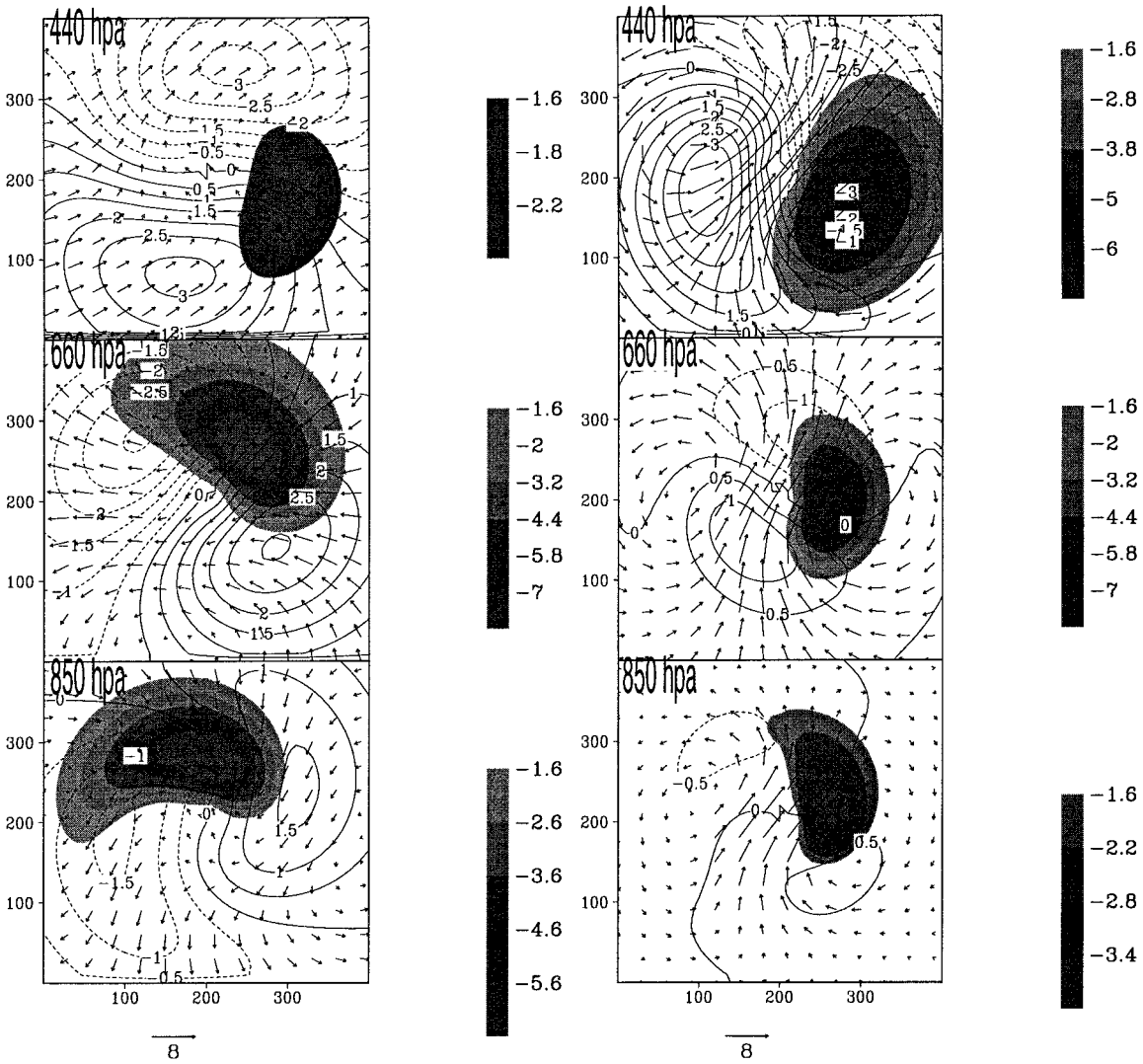

FIG. 9. Fields of vertical motion (*1.0 × 10^{-1} Pa^{-1}, shading), potential temperature (contours), and asymmetric flows relative to the TC motion at (top) 440, (middle) 660, and (bottom) 850 hPa at 48 h in (left panels) E1 and (right panels) E2. The intervals are 0.5 K for the potential temperature.

as shown in Fig. 9, the relative flow is southwesterly at 440 and 850 hPa. In this case, the maximum upward motion occurs upstream (downstream) of the relative flow at 440 (850) hPa. In other words, this mechanism leads to the maximum upward motion to the southwest (northeast) of the vortex center at 440 (850) hPa. Therefore, the combined effects of these two mechanisms can account for the vertical motion field at levels 660 and 850 hPa shown in Fig. 9.

To elucidate the relationship between the asymmetric vertical motion and the asymmetric potential temperature field, let us assume that the TC circulation is dominated by the symmetric and wavenumber-one components and that the asymmetric potential temperature fields observed in the coordinates moving with a TC are steady. This means that the local change of potential temperature caused by the horizontal advection ($-\mathbf{V}_1 \cdot \nabla\theta_s$ and $-\mathbf{V}_s \cdot \nabla\theta_1$) and vertical advection [$-\sigma_1(\partial\theta_s/\partial_\sigma)$] equals the potential temperature tendency associated with the TC motion ($-\mathbf{C} \cdot \nabla\theta_s$). By combining these terms, we have

$$\dot{\sigma}_1 \frac{\partial \theta_s}{\partial \sigma} \approx -\mathbf{V}_s \cdot \nabla\theta_1 - (\mathbf{V}_1 - \mathbf{C}) \cdot \nabla\theta_s, \qquad (5)$$

where θ_s and θ_1 are the symmetric and wavenumber-one potential temperature components, respectively. Equation (5) describes two physical mechanisms for the relationship between the asymmetric vertical motion and potential temperature fields.

The first mechanism, which is suggested by the first term on the right-hand side of Eq. (5), has been discussed in detail by Jones (1995) and Wang and Holland (1996a). Since θ_s always increases with height (decrease

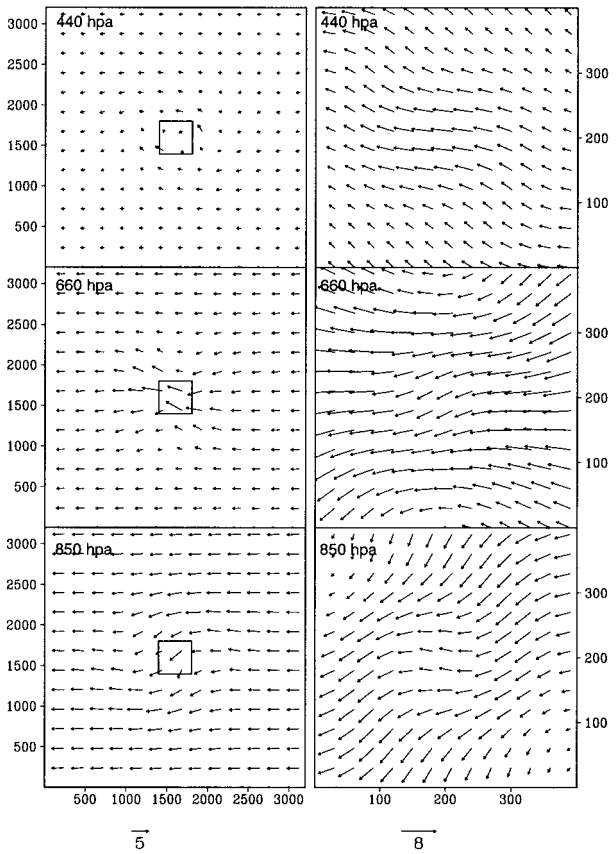

FIG. 10. The fields of the asymmetric flows on the (left panels) large scale and the (right panels) mesoscale at 440, 660, and 850 hPa at 48 h in E1. The domain is 3200 km × 3200 km in the left panels and 400 km × 400 km in the right panels.

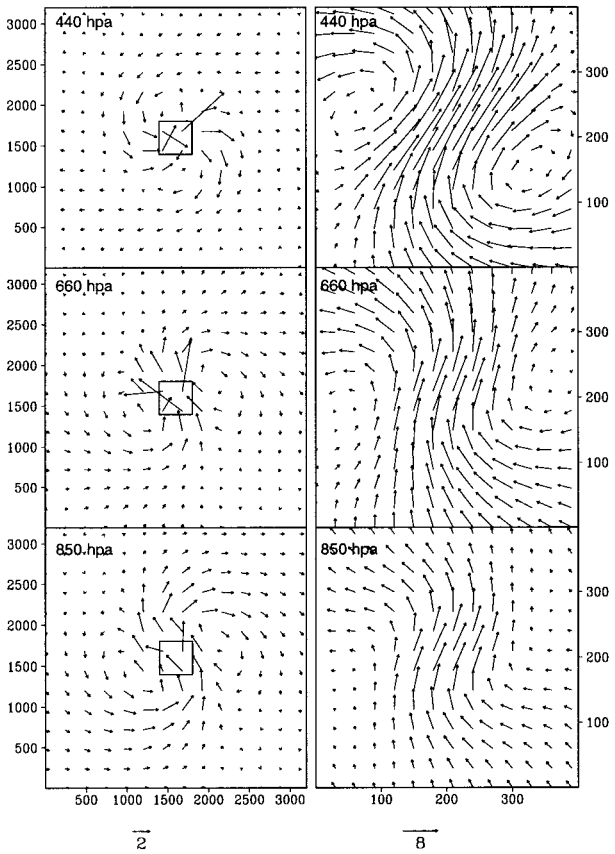

FIG. 11. The fields of the asymmetric flows on the (left panels) large scale and the (right panels) mesoscale at 440, 660, and 850 hPa at 48 h in E2. The domain is 3200 km × 3200 km in the left panels and 400 km × 400 km in the right panels.

with σ), a negative (positive) potential temperature anomaly corresponds to raised (lowered) isentropes. As an air parcel moves toward the region of lowered isentropes with the symmetric cyclonic flow, it must descend. As it moves back toward the raised isentropes, it must ascend. The maximum upward (downward) motion occurs between the positive and negative potential temperature anomalies. As suggested by Jones (1995), this mechanism suggests a 90° phase shift between the asymmetric potential temperature and the vertical motion fields. In E1 (Fig. 9), a phase shift of 90° between the potential temperature anomalies and the vertical motion fields occurs in the lower, middle, and upper troposphere.

In E2, however, the asymmetric potential temperature and vertical motion fields do not show such a phase shift (Fig. 9). In this case, the second mechanism, suggested by the term associated with the relative flow in Eq. (5), must be considered due to the strong relative flow in E2 (Fig. 9). As we know, the symmetric potential temperature component has its maximum at the vortex center due to the warm core of a TC. The second term suggests that an air parcel must descend (ascend) as it enters (leaves) the warm core. The ascending motion occurs downstream of the relative flow. In Fig. 9, the relative flows blow to the northeast of the vortex center in E2. A component of the upward motion to the northeast of the vortex center just accounts for the shift of the upward motion fields relative to the ones induced by the first mechanism. Since the relative flow over the vortex center in E1 is weak, this mechanism is not important in E1.

c. Inner gyres

The asymmetric flow in a TC has drawn much attention because it is closely associated with the TC motion. In Wang and Holland's (1996a) study, they suggest that, for a baroclinic vortex on a beta plane, the asymmetric flow arises from the beta gyres and the flow associated with the vertical projection of the tilted PV anomaly of a TC. In this study, we focus on the inner gyres, which have a smaller horizontal scale compared with the beta gyres.

Figure 10 shows the asymmetric wind fields at 48 h in E1. It can be seen that the initial zonal environmental flow was not affected too much by the baroclinic vortex, except in the region near the vortex centers, which is

shown in the right panels of this figure. Obviously, a mesoscale asymmetric wind field develops in the core region. In E2, on the large scale, the wind fields are dominated by the beta gyres, in which the two gyre centers are about 1000 km apart (Fig. 11). The pattern of the beta gyres at 660 and 850 hPa is very similar to that in barotropic models (e.g., Fioriono and Elsberry 1989). However, the flow in the core region is also dominated by two counter rotating gyres centered near the radius of maximum wind (the right panels).

It should be pointed out that the inner gyres resemble those found by Marks et al. (1992), especially when we look at them in the moving coordinate system (Fig. 11). Marks et al. analyzed the asymmetric wind fields with two National Oceanic Atmospheric Administration (NOAA) Aircraft Operation Center (AOC) WP-3D research aircraft. They documented a mesoscale asymmetric flow field relative to the TC motion, which is characterized by a wavenumber-one cyclonic/anticyclonic eddy couplet centered on the radius of maximum wind. As shown in Figs. 10 and 11, the inner gyres in E1 and E2 have those features, except that the distance from the gyre's center to the vortex center is relatively large in E1. The development of the inner gyres does not arise from the beta effect because we can also observe the inner gyres on an f plane (E1).

The development of the inner gyres is closely associated with the asymmetric PV component, P_1. The asymmetric wind fields develop in such a manner that the maximum combined effect of AASF and vertical PV advection is located upstream of the relative flow. For example, at 660 and 850 hPa, the maximum AASF is located upstream of the relative flow due to the relatively small effect of the vertical PV advection at these levels. Since both P_1 and σ_1 arise from the vertical tilt of the symmetric PV associated with a vortex, the inner gyres are also a result of the vertical tilt.

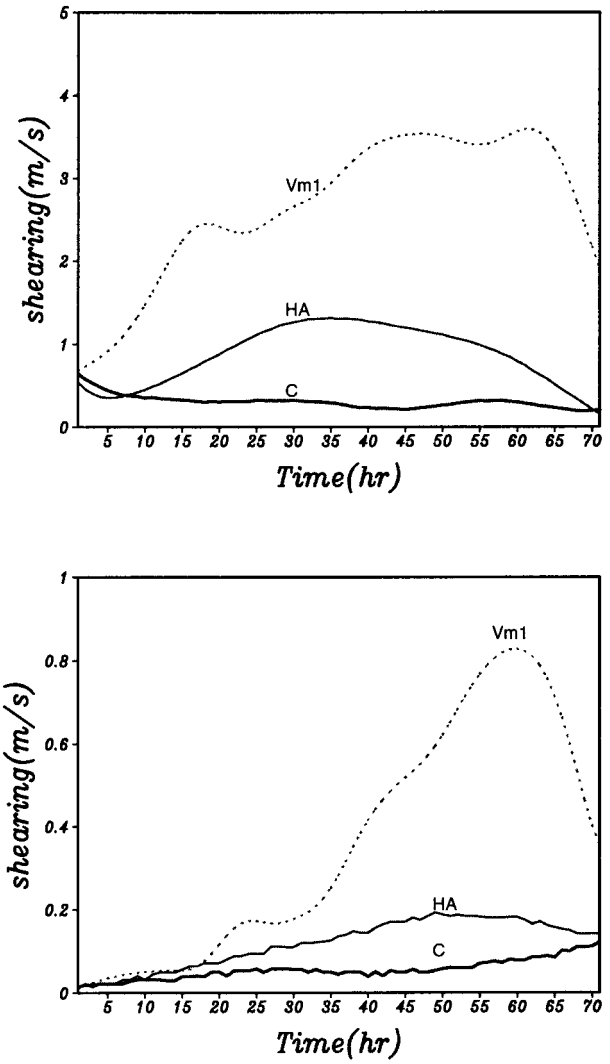

FIG. 12. The time series of the shearing index in (top) E1 and (bottom) E2. The **C**, $\mathbf{V}_{m1}$, and HA denote the real shearing, the shearings caused by the asymmetric flow, and the influence of horizontal PV advection.

5. Mechanisms of vertical coupling

Vertical coupling is the processes that prevent the TC centers at different levels from moving apart. In order to investigate the role of a physical process in vertical coupling, we define a shearing index (S), which is the rate at which the TC centers move apart. Here it is the magnitude of the velocity difference at 660 and 850 hPa, respectively. That is

$$S = \sqrt{(u_{660} - u_{850})^2 + (v_{660} - v_{850})^2}, \qquad (6)$$

where u_{660}, v_{850}, and v_{850} are the zonal and meridional TC speed components at 660 and 850 hPa. This index indicates the low-level vertical shearing that occurs in a TC. If the velocities denote the contribution of a specific physical process, the index also shows the influence of this process on the vertical coupling.

As discussed in section 3, there are three physical processes that may affect the vertical coupling: ASAF, AASF, and VA. Here we examine their individual roles in the vertical coupling by looking at how those processes affect the shearing index. Figure 12 shows the time series of the shearing index calculated in E1 and E2. One can find that the actual shearing in E1 remains almost constant at 0.3 m s^{-1}, while the index contributed from the mean asymmetric flow ($\mathbf{V}_{m1}$) varies remarkably with time. This situation is also found in E2. Although the actual shearing in E2 increases slowly with time, it is much smaller than that induced by the asymmetric flow ($\mathbf{V}_{m1}$) (Fig. 12). Thus, the influence of the asymmetric flow alone cannot account for the vertical coupling in E1 and E2.

Jones (1995) and Wang and Holland (1996a) explained the vertical coupling in terms of the penetration flow. According to Hoskins et al. (1985), the vertical penetration depth of a PV anomaly is directly propor-

tional to its strength, horizontal scale, and local frequency of rotation. This suggests that the penetration flows in E1 and E2 arise primarily from the lower-level anomaly because of the decrease of the cyclonic circulation with height in E1 and E2. It is also suggested that the penetration flow may be more intense in the inner core region because of the large local frequency of rotation. As expected, the asymmetric flow in the region inside the radius of maximum wind is indeed different from that in the outer region (Fig. 10). Considering that the vortex in E1 tilts northward at 48 h, the flow found in the eye appears to be the upward penetration flow in terms of the direction. In E2, however, such a penetration flow is not clear due to the relatively small vertical tilt. This suggests that the influence of the penetration flow on the vertical coupling is limited, especially in E2. This may arise from the absence of the upper-level anticyclone. We can conclude that neither the penetration flow nor the total asymmetric flow is enough to account for the vertical coupling in E1 and E2.

The role of the vertical PV advection in the vertical coupling is implied in Fig. 12. Its contribution is the difference between the contribution of HA and the actual shearing that occurs in E1 and E2. Clearly, the vertical PV advection also plays an important role in the vertical coupling. It should be noted that the vertical motion directly induced by the AASF cannot play a role in the vertical coupling, because its influence is perpendicular to the tilting plane. It is the vertical motion induced by the relative flow that contributes to the vertical coupling of the vortex. The influence of the vertical PV advection on the vertical coupling can be understood as follows. Consider the westerly (easterly) relative flow at the upper- (lower-) level. The vortex tilts eastward due to the shear of the relative flow. As mentioned in section 4, the upward (downward) motion is induced to the west (east) of the vortex. At the upper levels, the upward motion leads to a positive PV tendency or a motion component to the west of the vortex center. At the lower-level, on the other hand, the downward motion leads to a motion component to the east. Thus, the vertical advection associated with the relative flow can keep the vortex from tilting eastward.

In Fig. 12, the difference between the shearing due to $\mathbf{V}_{m1}$ and the shearing due to HA implies that the AASF also plays an important role in the vertical coupling in E1 and E2. The influence of AASF on the vertical coupling can be understood as follows. We take E1 as an example. At the beginning, the vortices at all levels move with the environmental flow because the influence of AASF associated with the environmental flow is small. Due to the westerly vertical shear of the environmental flow, the TC tilts eastward. The resulting vertical tilt induces a positive PV anomaly to the east (west) of the vortex center at 400 (850) hPa. As discussed above, the AASF associated with the PV anomalies induces asymmetric wind fields in such a way that the maximum AASF is located upstream of the relative flow. At 440 (850) hPa, we can see northerly (southerly) flow crosses the vortex in the coordinates moving with the TC. The induced relative flow, with the opposite directions at 440 and 850 hPa, would tilt the TC in the meridional direction. However, the influence of AASF leads to a northward (southward) motion, which reduces the vertical tilt caused by the meridional relative flow.

In summary, although the asymmetric flow over the TC core region may affect vertical coupling, most of the asymmetric flow may not result from the penetration flow in these two experiments. The AASF and VA can play an important role in the vertical coupling due to the vertical PV structure of a TC. Since the $\mathbf{V}_{m1}$, AASF and VA are all associated with the vertical tilt, their roles in the vertical coupling are inevitable results of the vertical tilt of an adiabatic baroclinic TC.

As we have seen, the roles of these physical processes in the vertical coupling arise from their opposite effects on the vortex motion above (below) the level with maximum PV. Therefore, the vertical structure of the symmetric PV component is critical to understanding the vertical coupling in E1 and E2. For E1 (Fig. 2), the level with maximum PV occurs at 850 hPa, and the vertical tilt is very small from the surface to the middle 660 hPa. In E2, the level with maximum PV occurs at 658 hPa. As a result, the circulation at the upper levels is still well aligned with the lower-level circulation.

6. Summary

Treated as a positive PV anomaly, the motion and vertical coupling of an initially symmetric baroclinic vortex were investigated in the absence of heating. The study was aimed at understanding the roles of various physical processes in TC motion and the mechanism by which a baroclinic TC maintains its coherent vertical structure. The baroclinic vortex moves under the influence of either the vertical sheared environmental flow or the differential beta drift.

In these two idealized cases, a baroclinic vortex that is initially symmetric will tilt in the vertical due to the vertical shear of the environmental flow or the differential beta drift. In response to this vertical tilt, a pair of asymmetric PV anomalies develops within this symmetric baroclinic vortex, with the positive asymmetric PV anomaly down-tilt (up-tilt) of the vortex above (below) the maximum PV level, in order to maintain a balance state between the thermal and dynamical fields. In association with the resulting asymmetric PV anomalies, a three-dimensional mesoscale asymmetric circulation develops. On the beta plane, in addition to the beta gyres, a pair of counterrotating inner gyres is found on the radius of maximum wind. This three-dimensional mesoscale asymmetric circulation has important influences on the movement and vertical coupling of adiabatic baroclinic vortices.

First, in the presence of the three-dimensional asym-

metric circulation, we cannot use only the horizontal advection of the symmetric PV component by the asymmetric flow to account for the TC motion. The TC motion is also determined by the advection of the asymmetric PV component by the symmetric flow and the vertical PV advection associated with the asymmetric vertical motion. Note that the horizontal advection of the symmetric PV component is also weighted by the horizontal gradient of the symmetric PV component.

The mesoscale inner gyres can have an influence on the vertical coupling, but most of the asymmetric flow does not arise from the penetration flow. Instead, we find that the counterrotating inner gyres are part of the three-dimensional asymmetric circulation induced by the vertical tilt of an initially symmetric baroclinic vortex. In addition, the advection of the asymmetric PV component by the symmetric flow and the vertical PV advection associated with the asymmetric vertical motion can also significantly contribute to the vertical coupling. The roles of these processes in the vertical coupling arise from the baroclinic structure of the symmetric PV component associated with TCs.

Although diabatic heating is of fundamental importance to the energetics of TCs, this adiabatic study is useful as a comparison to the diabatic study. Furthermore, due to the lack of sufficient deep convection, TCs often show relatively large vertical tilts in their early stage. In this case, the mechanisms discussed in this paper may play an important role in the movement and vertical coupling. Recently, Frank and Ritchie (1999) found that, in the early stages of moist simulations, the region of forced ascent and the associated mechanisms were similar to those in the dry runs. Nevertheless, for better insights into TC motion, understanding of the roles of diabatic heating in TC motion is definitely required since recent studies have shown that dry-adiabatic motions are not enough to describe the development of the vertical motion and coupling in moist TC-like vortices (e.g., Bender 1997; Frank and Ritchie 1999; Peng et al. 1999). In our future study, we will extend this work to include diabatic heating and reexamine the mechanisms for the movement and vertical coupling of baroclinic TCs.

Acknowledgments. We would like to thank two anonymous reviewers for their careful review and valuable comments, Dr. Y. Wang for giving us his original code of the hurricane model, and Mr. C. Orndorff for his comments. This research is supported by the Marine Meteorology Program of the Office of Naval Research. The International Pacific Research Center is sponsored in part by the Frontier Research System for Global Change.

REFERENCES

Bender, M. A., 1997: The effect of relative flow on the asymmetric structure in the interior of hurricanes. *J. Atmos. Sci.,* **54,** 703–724.

Carr, L. E., and R. L. Elsberry, 1990: Observational evidence for predictions of tropical cyclone propagation relative to steering. *J. Atmos. Sci.,* **47,** 542–546.

Dengler, K., and M. J. Reeder, 1997: The effects of convection and baroclinicity on the motion of tropical-cyclone-like vortices. *Quart. J. Roy. Meteor. Soc.,* **123,** 699–725.

Elsberry, R. L., 1995: Tropical cyclone motion. Global perspectives on tropical cyclones. WMO Tech. Doc. WMO/TD-693, 106–197.

Fiorino, M. J., and R. L. Elsberry, 1989: Some aspects of vortex structure related to tropical cyclone motion. *J. Atmos. Sci.,* **46,** 975–990.

Flatau, M., W. H. Schubert, and D. E. Stevens, 1994: The roles of baroclinic processes in tropical cyclone motion: The influence of vertical tilt. *J. Atmos. Sci.,* **51,** 2589–2601.

Frank, W. M., and E. A. Ritchie, 1999: Effects of environmental flow upon tropical cyclone structure. *Mon. Wea. Rev.,* **127,** 2044–2061.

Franklin, J. L., S. E. Feuer, J. Kaplan, and S. D. Aberson, 1996: Tropical cyclone motion and surrounding flow relationship: Searching for beta gyres in Omega dropwindsonde datasets. *Mon. Wea. Rev.,* **124,** 64–84.

Hoskins, B. J., M. E. Mcintyre, and A. W. Robertson, 1985: On the use and significance of isentropic potential vorticity maps. *Quart. J. Roy. Meteor. Soc.,* **111,** 877–946.

Jones, S. C., 1995: The evolution of vortices in vertical shear. Part I: Initially barotropic vortices. *Quart. J. Roy. Meteor. Soc.,* **121,** 821–851.

Marks, F. D., Jr., R. A. Houze Jr., and J. F. Gamache, 1992: Dual-aircraft investigation of the inner core of Hurricane Norbert. Part 1: Kinematic structure. *J. Atmos. Sci.,* **49,** 919–942.

Peng, M. S., B.-F. Jeng, and R. T. Williams, 1999: A numerical study on tropical cyclone intensification. Part I: Beta effect and mean flow effect. *J. Atmos. Sci.,* **56,** 1404–1423.

Raymond, D. J., 1992: Nonlinear balance and potential-vorticity thinking at large Rossby number. *Quart. J. Roy. Meteor. Soc.,* **118,** 987–1015.

Shapiro, L. J., 1992: Hurricane vortex motion and evolution in a three-layer model. *J. Atmos. Sci.,* **49,** 140–153.

Wang, B., and X. Li, 1992: The beta drift of three-dimensional vortices: A numerical study. *Mon. Wea. Rev.,* **120,** 579–593.

Wang, Y., 1995: Baroclinic aspects of tropical cyclone motion. Ph.D. thesis, Monash University, 268 pp.

——, 1998: On the bogusing of tropical cyclones in numerical models: The influence of vertical structure. *Meteor. Atmos. Phys.,* **65,** 153–170.

——, and G. J. Holland, 1996a: The beta drift of baroclinic vortices. Part I: Adiabatic vortices. *J. Atmos. Sci.,* **53,** 411–427.

——, and ——, 1996b: The beta drift of baroclinic vortices. Part II: Diabatic vortices. *J. Atmos. Sci.,* **53,** 3737–3756.

——, and ——, 1996c: Tropical cyclone motion and evolution in vertical shear. *J. Atmos. Sci.,* **53,** 3313–3332.

Wu, C.-C., and K. A. Emanuel, 1993: Interaction of a baroclinic vortex with background shear: Application to hurricane movement. *J. Atmos. Sci.,* **50,** 62–76.

——, and ——, 1995a: Potential vorticity diagnostics of hurricane movement. Part I: A case study of Hurricane Bob (1991). *Mon. Wea. Rev.,* **123,** 69–92.

——, and ——, 1995b: Potential vorticity diagnostics of hurricane movement. Part II: Tropical Storm Ana (1991) and Hurricane Andrew (1992). *Mon. Wea. Rev.,* **123,** 93–109.

Wu, L., and B. Wang, 1999: Numerical study of tropical cyclone propagation in the presence of diabatic heating. Preprints, *23d Conf. on Hurricanes and Tropical Meteorology,* Dallas, TX, Amer. Meteor. Soc., 91–94.

——, and ——, 2000: A potential vorticity tendency diagnostic approach for tropical cyclone motion. *Mon. Wea. Rev.,* **128,** 1899–1911.